Journal of proteome research

Article

pubs.acs.org/jpr

Metabolomic Analysis of Siderophore Cheater Mutants Reveals Metabolic Costs of Expression in Uropathogenic *Escherichia coli*

Haitao Lv,*[,†,‡,§] Chia S. Hung,[†] and Jeffrey P. Henderson*[,†]

[†]Center for Women's Infectious Diseases Research, Division of Infectious Diseases, Department of Medicine, Washington University School of Medicine, St. Louis, Missouri 63110, United States

[‡]Chongqing University Innovative Drug Research Center, Chongqing 401331, P. R. China

[§]Tissue Repair and Regeneration Program, Institute of Health and Biomedical Innovation, Queensland University of Technology, Kelvin Grove, QLD 4059, Australia

Supporting Information

ABSTRACT: Bacterial siderophores are a group of chemically diverse, virulence-associated secondary metabolites whose expression exerts metabolic costs. A combined bacterial genetic and metabolomic approach revealed differential metabolomic impacts associated with biosynthesis of different siderophore structural families. Despite myriad genetic differences, the metabolome of a cheater mutant lacking a single set of siderophore biosynthetic genes more closely approximate that of a non-pathogenic K12 strain than its isogenic, uropathogen parent strain. Siderophore types associated with greater metabolomic perturbations are less common among human isolates, suggesting that metabolic costs influence success in a human population. Although different siderophores share a common iron acquisition function, our analysis shows how a metabolomic approach can distinguish their relative metabolic impacts in *E. coli*.

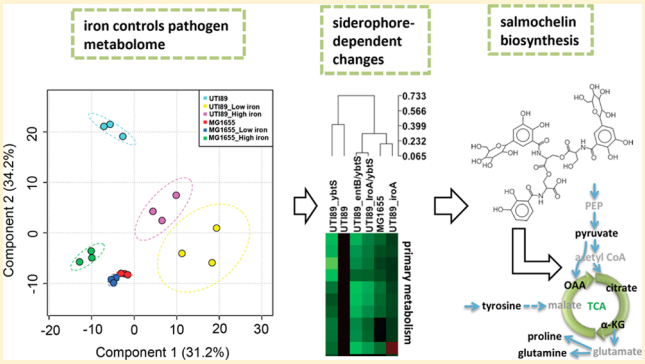

KEYWORDS: *metabolomics, siderophores, primary metabolism, salmochelin, uropathogenic Escherichia coli, metabolic cost*

INTRODUCTION

Extraintestinal pathogenic *Escherichia coli* (ExPEC) pathotypes express genes that help them to occupy anatomic and environmental locations both inside and outside the gastrointestinal tract. Compared to K12 strains, uropathogenic *E. coli* (UPEC) carry an expanded repertoire of iron-regulated genes.[1,2] These nonconserved or plasmid-bourne genes encode transporters, adhesins, toxins, and biosynthetic proteins that produce ferric ion chelators called siderophores.[3−11] Siderophores are a chemically diverse group of specialized metabolites defined by their ability to bind scarce ferric ions to yield a ferric complex that is preferentially used as a bacterial nutritional source.[12,13] It is an enduring curiosity that *E. coli* and other bacteria often express multiple, independent siderophore systems.[8] Although siderophore production can aid bacterial growth, production of these and other virulence-associated products has also been proposed to exact biologically important metabolic costs.[14] These costs have been proposed to explain the existence of naturally arising siderophore biosynthetic mutants (also known as "cheater" strains) that nonetheless retain their ability to use siderophore-associated iron generated by other strains.[8] While some siderophores may confer important gains-of-function in specific microenvironments,[15,16] their associated metabolic costs may be maladaptive in environments in which they are functionally redundant.

To relate virulence genes to metabolism, we combined a bacterial genetic approach with mass-spectrometry-based metabolomics. This metabolomic analysis measured variations in 44 established *E. coli* primary metabolites present in all known strains using targeted liquid chromatography−mass spectrometry (LC−MS/MS)[8,10] (Figure 1). Compared to untargeted metabolomic profiling, this approach yields higher quality quantitative data on primary metabolites common to all known *E. coli* isolates. We overviewed the resulting metabolite data matrices using principal components analysis (PCA),[17] an unsupervised multivariate analysis. In these PCA plots, each bacterial metabolome is represented as a point plotted near bacteria with similar metabolomes and farther away from bacteria with less similar metabolomes. This permits relative quantification of metabolomes associated with different strains and/or culture conditions. In this study we observed substantial iron-induced metabolomic changes in a pathogen that were traced to biosynthesis of a single siderophore type. The overall

Received: September 24, 2013
Published: January 30, 2014

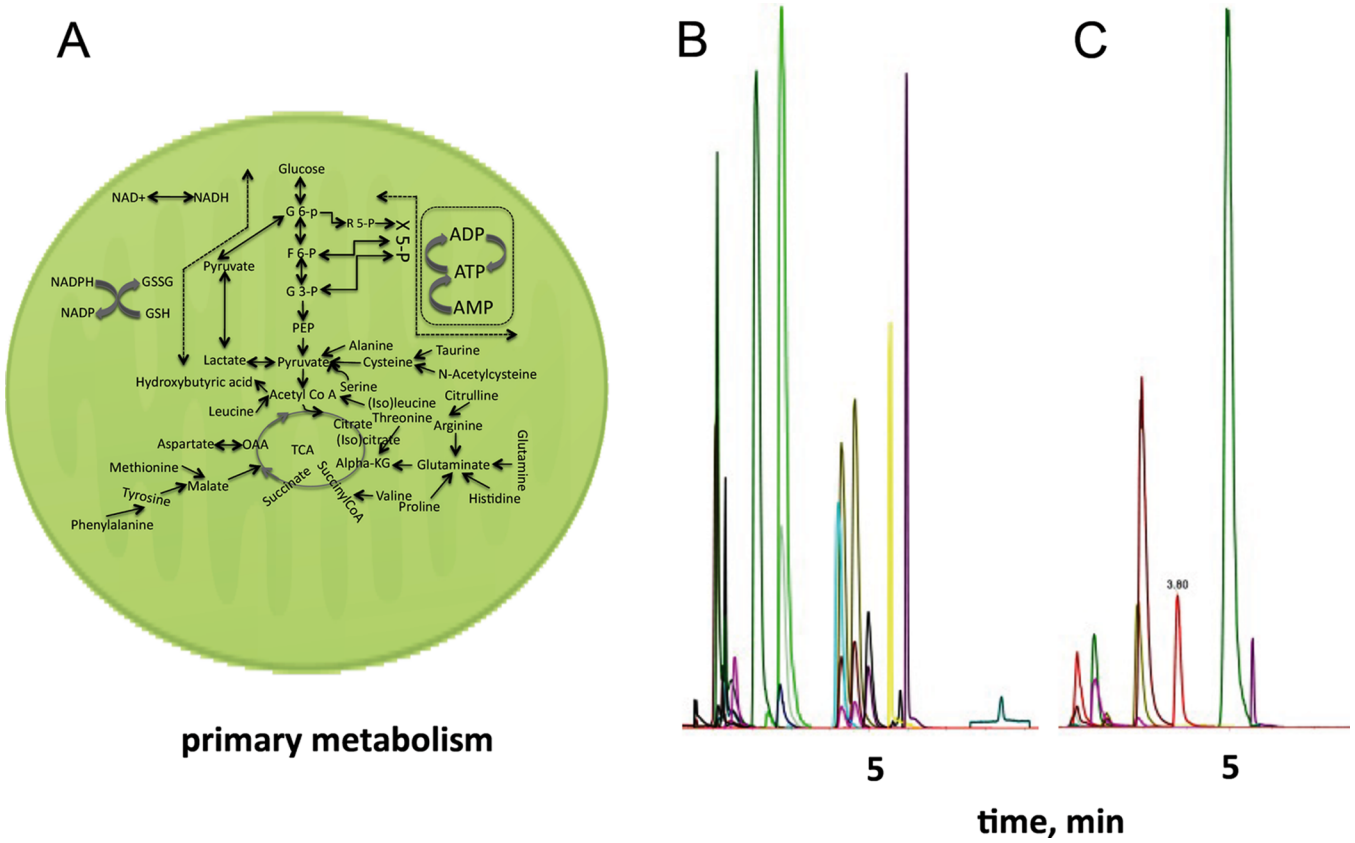

Figure 1. Profiling of primary metabolism of pathogenic and non-pathogenic *E. coli* by LC−MS/MS-based targeted metabolomics approach. (A) The primary metabolites hosted by the targeted metabolic pathways such as TCA cycle, glycolysis, gluconeogenesis, pentose phosphate pathway, and amino acid metabolism. (B, C) LC−MS metabolic profiling of primary metabolites in multiple monitoring reaction modes of positive (ESI+) and negative (ESI−).

approach can be readily adapted to explore other virulence-associated bacterial products.

RESULTS

Iron Restriction Reveals Strain-Dependent Metabolomic Shifts

To determine whether iron availability affects the *E. coli* primary metabolome, we cultured the model non-pathogenic K12 strain MG1655 and the model uropathogen UTI89 in media containing different iron levels. These bacteria were grown in a standard culture condition known to induce disease-associated levels of siderophore expression while permitting uniform growth between strains (Figure 1, Supplementary Figure 1). To confirm that the cultured bacteria sensed these differences in iron availability, we monitored siderophore production, which is repressed by ferric uptake repressor (Fur) when iron is abundant and derepressed when it is scarce. Stable isotope dilution LC−MS/MS measurements in both strains revealed production of the conserved *E. coli* siderophore enterobactin at low (0.162 mg/L) or absent supplemental iron. UTI89 also produced the additional, virulence-associated siderophores yersiniabactin[15] and salmochelin[18] under the standard growth condition (Figure 2A). All siderophore production was suppressed by both strains in the high iron supplementation condition (16.2 mg/L, Figure 2B) as expected. Iron supplementation only modestly increased growth (Supplementary Figure 1). Altogether, these observations are consistent with a standardized, subtoxic range of iron supplementation that modulates *E. coli* iron scarcity responses.

Next, we sought to determine whether iron availability affects steady state primary metabolite levels (the primary metabolome) in these strains. PCA of the same primary metabolites from MG1655 and UTI89 cultured in the three iron conditions revealed larger iron-dependent shifts in UTI89 than in MG1655 (Figure 2C). Strikingly, while the largest iron-induced shift was observed in UTI89 with low-level iron supplementation (Figure 3), the same iron supplementation in MG1655 resulted in the smallest metabolomic shift (Figure 2C). Low-level iron supplementation slightly stimulated enterobactin and salmochelin in UTI89, while slightly lowering yersiniabactin levels (Figure 3B). These data show that iron availability can affect the primary metabolome but that it does so in a strain-dependent manner (Figure 3). This striking difference in primary responses likely derives from differences in iron-responsive genetic systems between these two strains.

Siderophore Biosynthesis Causes Iron- and Strain-Dependent Metabolomic Shifts

To determine whether siderophore biosynthetic differences contribute to strain-dependent metabolomic differences, we used PCA to compare MG1655 to a panel of UTI89 siderophore biosynthesis mutants (Table 1). As shown in Figure 4A, principal component 1 (PC1) explained 40.2% of variance among these strains, with PC2 explaining only 12.7%. Wild type MG1655 and UTI89 were the extremes in this analysis, exhibiting the greatest difference predominantly along

dx.doi.org/10.1021/pr4009749 | J. Proteome Res. 2014, 13, 1397−1404

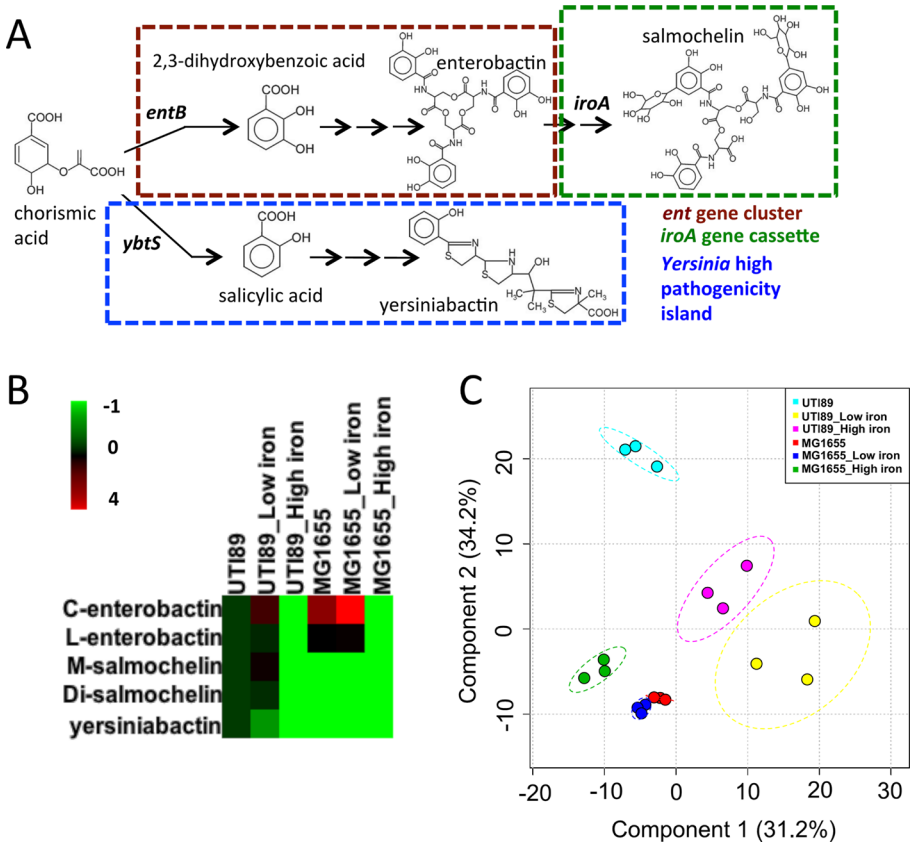

Figure 2. Iron limitation differentially affects pathogenic and non-pathogenic *E. coli* primary metabolomes. (A) Biosynthetic pathways for conserved *E. coli* siderophore enterobactin and the two additional siderophores produced by the model uropathogen UTI89. (B) Heat map depicting relative siderophore production for UTI89 and the non-pathogenic K12 strain MG1655 with no, low (0.162 mg/L), and high (16.2 mg/L) iron-supplemented growth conditions. Cyclic and linearized enterobactin (C-enterobactin and L-enterobactin), salmochelin (in its mono- and diglycosyl forms, denoted by prefixes M and Di, respectively), and yersiniabactin were quantified using stable isotope dilution LC–MS/MS. Siderophore suppression during high iron growth is evident in UTI89. (C) Principal components analysis (PCA) scatter plot of cell-associated primary metabolites reveals marked iron-dependent metabolomic shifts in UTI89.

the PC1 dimension. Compared to UTI89, the complete siderophore-null strain UTI89Δ*entB*Δ*ybtS* exhibited a marked metabolomic shift along the first principal component to closely approximate MG1655. Notably, the UTI89Δ*entB*Δ*ybtS* metabolome more closely resembled that of MG1655 than the wild type UTI89 parent strain. This finding is consistent with siderophore biosynthesis as a major contributor to the UTI89-MG1655 metabolomic difference (Figure 4B). Because MG1655 expresses enterobactin, salmochelin or yersiniabactin biosyntheses emerge as major candidate contributors to the primary metabolomic difference between strains (Supplementary Figures 2–4).

The metabolomic impacts of salmochelin and yersiniabactin are more directly assessed with the siderophore biosynthetic mutants UTI89Δ*entB*Δ*ybtS*, UTI89Δ*iroA*Δ*ybtS*, UTI89Δ*iroA*, and UTI89Δ*ybtS* (Figure 4C). Consistent with previous observations,[10] the yersiniabactin-null UTI89Δ*ybtS* mutant is least affected. The other mutants (UTI89Δ*entB*Δ*ybtS*, UTI89Δ*iroA*Δ*ybtS*, UTI89 Δ*iroA*) share a common salmochelin biosynthetic deficiency phenotype (Figure 4A) and are the three most similar strains in this analysis. Although these strains are deficient in either early or late stages of salmochelin biosynthesis (Δ*entB* and Δ*iroA*, respectively, Figure 4A), their primary metabolomes were more similar to MG1655 than to UTI89 (Figures 4B). These results support salmochelin biosynthesis as a primary contributor to the marked metabolomic divergence between uropathogenic and non-pathogenic *E. coli* (Figure 4C).

Metabolomic Impact Is Inversely Associated with Siderophore Expression Frequency in Cystitis Isolates

These results show that the magnitude of siderophore-associated primary metabolic shifts varies widely between each of three different siderophore types (Figure 4). Because a larger metabolomic perturbation might negatively impact fitness, we reviewed each siderophore's abundance in a clinical *E. coli* strain collection.[8] Among the three siderophores examined here, expression frequency in cystitis strains is 50% for salmochelin, 71% for yersiniabactin, and 100% for enterobactin. In commensal isolates from the same patients, enterobactin expression remained at 100%, while salmochelin and yersiniabactin dropped to 13% and 31%, respectively. Siderophore expression frequencies were thus negatively correlated with the magnitude of their metabolomic perturbations such that the least common siderophore (salmochelin) was associated with the largest metabolomic shift (Figure 4). Of note, salmochelin exhibited the widest expression range, with commensal isolates expressing lower levels than coexisting pathogens. Although salmochelin expression may facilitate pathogenesis, these data suggest that its high metabolic cost may be a consequential disadvantage to *E. coli* occupying non-pathogenic niches (Figure 4). Conversely, maintenance of this metabolically expensive pathway in a population suggests that it

dx.doi.org/10.1021/pr4009749 | *J. Proteome Res.* 2014, 13, 1397–1404

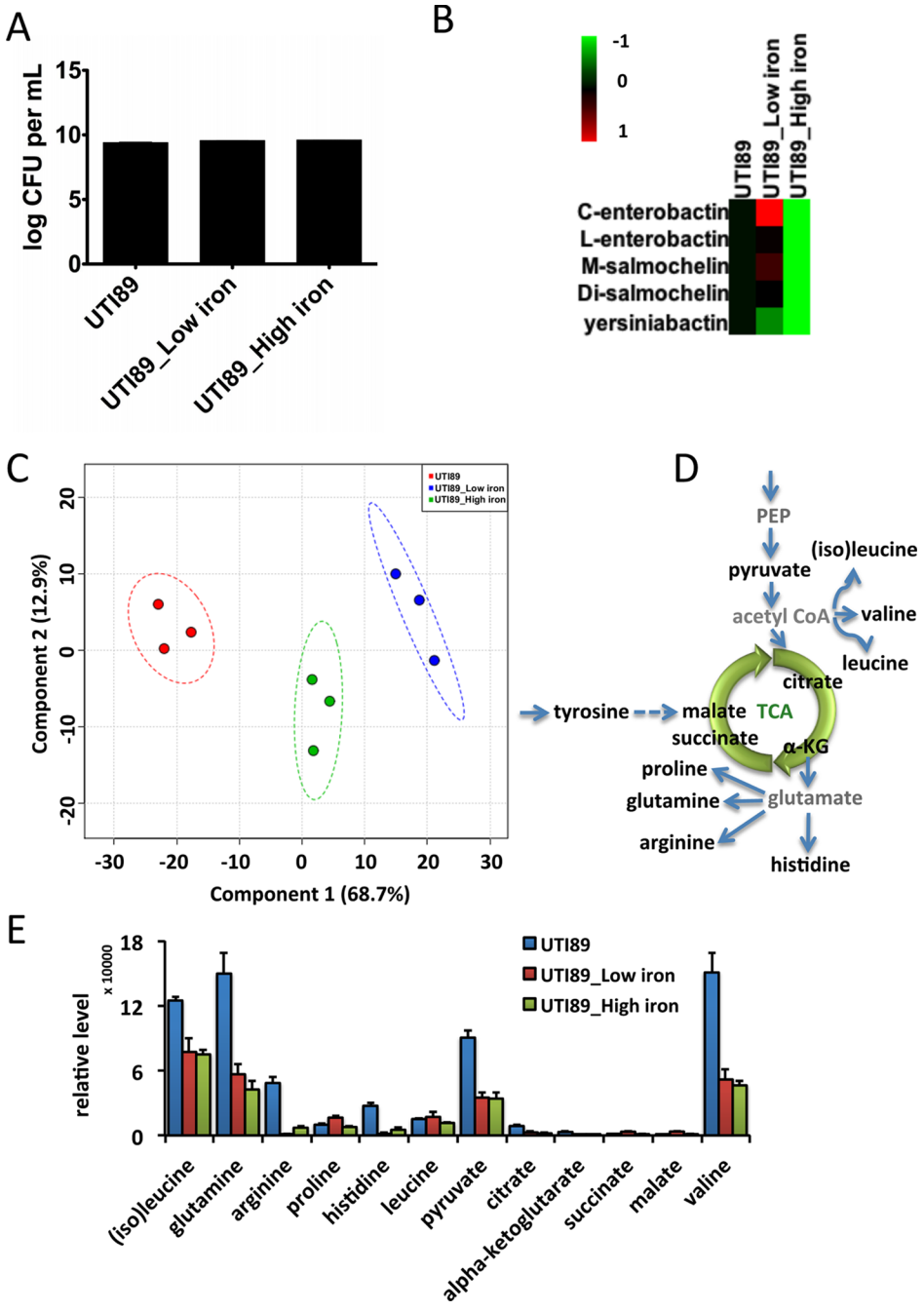

Figure 3. Iron regulates both siderophore production and primary metabolism. (A) Iron modestly increases 18 h growth of uropathogenic *E. coli* strain UTI89 as assessed by live cell density (CFU/mL). (B) Heat map depicting relative siderophore production by UTI89 following growth in culture media supplemented with no, low (0.162 mg/L), or high (16.2 mg/L) ferric chloride. Cyclic and linearized enterobactin (C-enterobactin and L-enterobactin), salmochelin (in its mono- and diglycosyl forms, denoted by prefixes M and Di, respectively), and yersiniabactin were quantified using stable isotope dilution LC–MS/MS. (C) PCA resolves iron-dependent metabolomic groupings in UTI89. (D) Primary metabolites affected by iron supplementation and their relationships to the TCA cycle, glycolysis, and amino acid metabolism. (E) Bar plots for differential metabolites derived from the affected metabolic pathways by VIP analysis.

Table 1. Siderophores Expressed by *E. coli* Strains in This Study

	enterobactin	linear enterobactin	salmochelin (monoglucose)	salmochelin (diglucose)	yersiniabactin	refs
UTI89	+	+	+	+	+	8
UTI89Δ*ybtS*	+	+	+	+		8, 10, 36
UTI89Δ*iroA*	+	+			+	8, 22
UTI89Δ*iroA*Δ*ybtS*	+	+				8
UTI89Δ*entB*Δ*ybtS*						8, 37
MG1655 (K12)	+	+				8, 10

dx.doi.org/10.1021/pr4009749 | *J. Proteome Res.* 2014, 13, 1397–1404

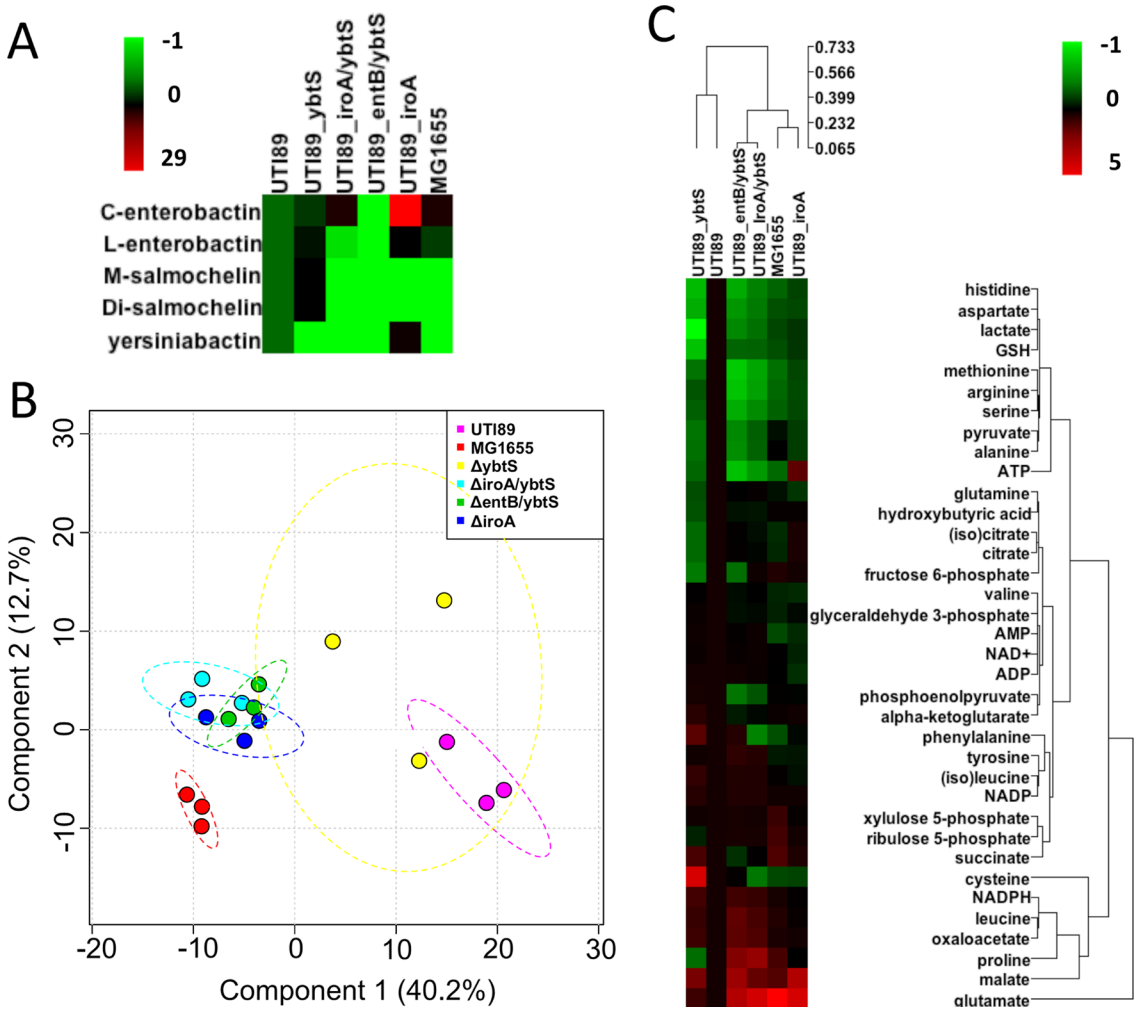

Figure 4. Pathogen-associated primary metabolomic differences derive primarily from the salmochelin biosynthetic pathway. (A) Relative siderophore production confirms salmochelin production by UTI89 and UTI89Δ*ybtS* but not MG1655 or UTI89 mutants lacking *entB* or *iroA*. (B) PCA of the primary metabolome reveals that the UTI89 metabolome is affected similarly by loss of *entB* and *iroA* and that loss of these genes causes the metabolome to approximate that of non-pathogenic MG1655. (C) Heat map of primary metabolites normalized to wild type UTI89 levels. Hierarchical clustering analysis produces a dendrogram in which the presence of an intact salmochelin biosynthetic pathway, rather than pathogen or non-pathogen strain background, is the primary discriminant.

may play a highly unique adaptable role in certain environments.

DISCUSSION

Previous genetic, transcriptional, and proteomic analyses have indicated that uropathogenic *E. coli* respond to iron scarcity in a multifaceted manner.[1,19,20] This study shows how metabolomics can be combined with traditional microbiological approaches to identify biosynthetic functions that disproportionately impact complex metabolic networks. While our findings that uropathogenic and K12 *E. coli* metabolomes respond differently to iron restriction might have been predictable, the disproportionate impact of one virulence-associated genetic system, salmochelin biosynthesis, is striking. Among the factors affecting siderophore expression costs are the specific costs of synthesizing each siderophore, the number of siderophores produced, energy used to transport siderophores, and the ability to recycle siderophores or siderophore products following uptake. Compared to enterobactin, salmochelin production requires UDP-glucose consumption from the gluconeogenesis pathway.[11,21,22] Furthermore, while the serine and dihydroxybenzoic acid (DHBA) degradation products generated following ferric enterobactin uptake might be reused, the glucosyl-DHBA product released following ferric-salmochelin may be not be a substrate for reincorporation. These factors may alter flux through many metabolic pathways, leading to the multiple salmochelin-associated changes in the steady state primary metabolome observed here (Figure 5).

Salmochelin's metabolomic impact raises the question of why this siderophore system persists in uropathogenic *E. coli* populations. Two functional advantages described for salmochelin expression concern its ability to evade sequestration by cell membranes[9] and to evade binding to lipocalin-2,[23] a siderophore-binding innate immune protein. While other siderophore functions are conceivable,[15,16] salmochelin-expressing *E. coli* exhibit lipocalin-2-dependent virulence of in a mouse septicemia model, suggesting an important role for iron acquisition.[24] Overall, salmochelin expression may confer a selective advantage in some host niches that is sufficient to overcome the detrimental metabolomic consequences of its expression.

dx.doi.org/10.1021/pr4009749 | *J. Proteome Res.* 2014, 13, 1397−1404

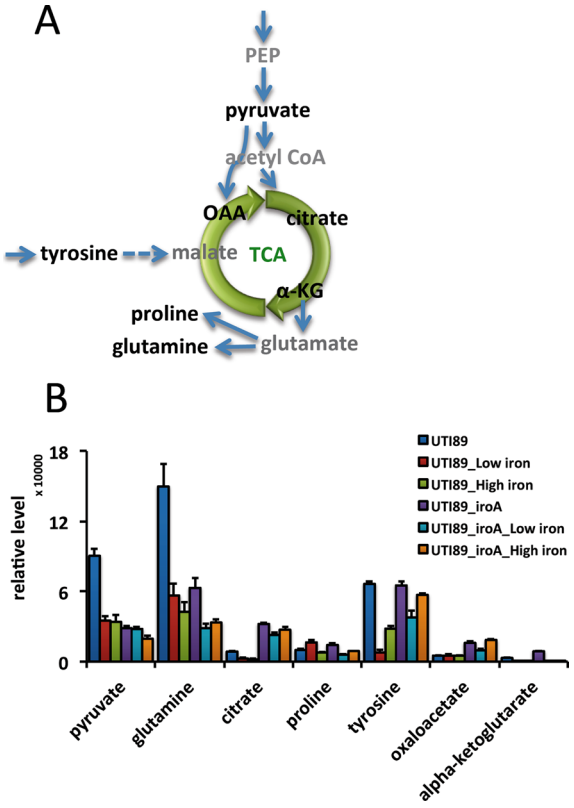

Figure 5. Primary metabolites whose variations correspond to salmochelin expression. (A) Primary metabolites in UTI89 affected by iron supplementation and salmochelin expression (in black lettering) identified by VIP analysis and their relationships to the TCA cycle, glycolysis, and amino acid metabolism. (B) Primary metabolite levels for selected metabolites differentiating UTI89 from UTI89ΔiroA.

A similar metabolomics/bacterial genetics approach could be adapted to identify analogous relationships in other pathogens. Analogous metabolic penalties may explain why some *Pseudomonas* strains spontaneously stop expressing the siderophore pyochelin during long-term lung colonization in cystic fibrosis patients.[25,26] Identifying gene-associated metabolic burdens may also provide insight into antivirulence genes in bacterial pathogens, which must be inactivated for full expression of a pathogenic phenotype.[27]

While steady state metabolomic analysis provides an analytically robust approach to identifying metabolomic alterations, definitively tracing these alterations to specifically altered pathways will require additional approaches. Metabolic flux analysis ("fluxomics") may permit analyses such as these and could reconcile salmochelin biosynthesis with changes in specific metabolic pathways.[28]

MATERIALS AND METHODS

Chemicals and Reagents

Acetonitrile (HPLC grade), formic acid (LC/MS grade), and water (LC/MS grade) were purchased from Fisher Scientific (Fisher Scientific, Pittsburgh, PA, USA); the standard compounds of NAD+, NADH, NADP, NADPH, AMP, ADP, ATP, ribulose 5-phosphate (R 5-P), xylulose 5-phosphate (X 5-P), fructose 6-phosphate (F 6-P), glyceraldehyde 3-phosphate (G 3-P), phosphoenolpyruvate (PEP), lactate, pyruvate, citrate, (iso)citrate, alpha-ketoglutarate (alpha-KG), succinate, malate, oxaloacetate (OAA), aspartate, glutaminate, glutamine, reduced glutathione (GSH), oxidized glutathione (GSSG), (iso)leucine, leucine, alanine, arginine, cysteine, methionine, proline, serine, threonine, tyrosine, phenylalanine, valine, histidine, *N*-acetylcysteine, and hydroxybutyric acid were purchased from Sigma (Sigma-Aldrich Corp., Saint Louis, MO, USA). All other reagents were ACS grade.

Bacterial Strains and Culture

Bacteria were routinely cultured in LB broth, and metabolites were analyzed following 18 h of growth in an established M63 minimal medium condition with glycerol as the carbon source.[8,10,29] Deletion mutants were made using the previously described red recombinase method with pKD4 or pKD13 as a template and confirmed by PCR with flanking primers.[8,30,31] Antibiotic insertions were removed by transforming the mutant strains with pCP20 expressing the FLP recombinase.[32]

Metabolite Extraction

Cell pellets were isolated from 50 mL of culture solution, fast-quenched with ice-cold methanol by spinning down to 11,500 × *g* at 4 °C for 10 min, mixed with 1.2 mL of 80% ice-cold methanol by vortexing for 30 s, and kept on dry ice for 30 min. Next, 20 dounces of homogenization were performed, and the sample was centrifuged at 23,008 × *g* at 4 °C for 10 min. The supernatant was then mixed with 800 μL of ice-cold acetonitrile for 15 min before lyophilization. Prior to analysis, the dried sample was dissolved in 1 mL of water, and 5 μL was analyzed by LC−MS. All above procedures should be performed within safety hood.

Siderophore Extraction

Twelve microliters of 0.1 M ferric chloride and 50 μL of ^{13}C-labeled internal standard[8] were added to 2 mL of cell supernatant to a final concentration of 0.1 mM. After 15 min of room temperature incubation, the precipitate was removed by centrifugation. The supernatant was applied to a 96-well SPE plate (United Chem Inc., PA, USA) with 50 mg of DEAE media per well that was preconditioned with 0.5 mL of methanol and 0.5 mL of water. Each well was washed with 0.5 mL of water, and siderophores were eluted with 0.5 mL of 7.5 M ammonium formate (pH 3.6). Ten microliters of elute was injected into the LC−MS instrument for siderophore analysis.

Ultrafast Liquid Chromatography−Mass Spectrometry (LC−MS)

Previously described LC−MS/MS analytical platforms were introduced to analyze intracellar hydrophilic metabolites and siderophore molecules expressed in bacterial cells.[8,10]

Ultrafast liquid chromatography (UFLC) (Shimadzu, Kyoto, Japan) consisted of two LC-20AD XR pumps, a DGU-20A3 prominence vacuum degasser, an SIL-20AXR autosampler, a CTO-20A prominence column oven, and a CBM-20A communications bus module, coupled with a hybrid API 4000 Qtrap (AB Sciex, Foster City, CA, USA) with an Turbo V ESI ionization source interface, and a computer platform equipped with a Solution Analyst software version 1.5.1 (AB Sciex, Foster City, CA, USA) was used for data acquisition and preprocessing. Targeted metabolomics analysis of hydrophilic metabolites was performed on a Acquity HSS T3 column (150 mm × 2.0 mm, 1.7 μm, Waters) using a gradient of 0−27% B over 8 min, then B increase to 99% from 8 to 10 min (A: 0.1% formic acid in water; B: 0.1% formic acid in acetonitrile) at a flow rate of 0.3 mL/min. The samples were analyzed by a UFLC−MS system in positive or negative ionization modes

dx.doi.org/10.1021/pr4009749 | J. Proteome Res. 2014, 13, 1397−1404

with an electrospray ionization voltage of 5500 V for positive mode and 4500 V for negative mode, nebulizer gas (air) and turbo gas (air) settings at 50 and 50 psi, and a turbosource gun temperature of 500 C. The curtain gas (nitrogen) was set at 25 psi, and the collision cell pressure at low or high mode for different purposes. The MRM parameter for each metabolite is recorded in reference.[10]

LC−MS determination of siderophores was performed on a Betasil C18 Column (50 mm × 2.1 mm, 5.0 μm, Thermo Scientific) with a gradient as follows: 2.0−65% B over 10 min (A: 0.1% formic acid in water; B: 0.1% formic acid in acetonitrile) at a flow rate of 0.4 mL/min. MRM parameters are listed in ref 8 (Supplementary Figure 5).

Chemometric Analysis

Normalization of relative peak area, pattern recognition analysis with unsupervised principal component analysis (PCA) was performed using the Metaboanalyst web based metabolomics platform (www.metaboanalyst.ca).[33,34] The resulted scatter score plot was utilized to reveal the similarity or difference between or among groups, and the loading plot (VIP plot) was used to identify differentiable metabolites with marked contribution to group classification. Heatmap overviews of the data were generated using an FDA Genomic Tool (ArrayTrack).[35] For siderophore expression, the relative level of each siderophore was calculated by peak area of siderophore/peak area of isotope-labeled siderophore, then the heatmap was plotted without further normalization, and median-centered data were used for hierarchical clustering analysis using Ward's Minimum Variance method (Euclidian-Ward, autoscaled). For primary metabolism comparison, the normalized peak areas of primary metabolites underwent further normalization with $\log_{10}$ transformation before the heatmap was plotted, and median-centered data were used for hierarchical clustering analysis using Ward's Minimum Variance method (Euclidian-Ward, autoscaled).

Statistical Analyses

Bar plot graphs and all other statistics were generated using GraphPad Prism 5.0 and Microsoft Excel.

■ ASSOCIATED CONTENT

Supporting Information

This material is available free of charge via the Internet at http://pubs.acs.org.

■ AUTHOR INFORMATION

Corresponding Authors

*Phone: 086-23-65678464. Fax: 086-23-65678450. E-mail: haitao.lu@cqu.edu.cn.

*Phone: 01-314 454-8225. Fax: 01-314 454-5392. E-mail: jhenderson@borcim.wustl.edu.

Notes

The authors declare no competing financial interest.

■ ACKNOWLEDGMENTS

J.P.H. is supported by a Career Award for Medical Scientists from the Burroughs Wellcome Fund. Funding was also provided by National Institutes of Health grants HD001459-09, UL1 RR024992, HL101263-01, and DK064540. H.L. is supported by Natural Science Foundation of China grant 81274175, the QUT Vice Chancellor's Research Fellowships Grant 150410-0070/08, Startup Funding for "Hundred Young-Talent Scheme" provided by Chongqing University in China 0236011104401.

■ REFERENCES

(1) Chen, S. L.; Hung, C. S.; Xu, J.; Reigstad, C. S.; Magrini, V.; Sabo, A.; Blasiar, D.; Bieri, T.; Meyer, R. R.; Ozersky, P.; Armstrong, J. R.; Fulton, R. S.; Latreille, J. P.; Spieth, J.; Hooton, T. M.; Mardis, E. R.; Hultgren, S. J.; Gordon, J. I. Identification of genes subject to positive selection in uropathogenic strains of Escherichia coli: a comparative genomics approach. *Proc. Natl. Acad. Sci. U.S.A.* **2006**, *103* (15), 5977−82.

(2) Cusumano, C. K.; Hung, C. S.; Chen, S. L.; Hultgren, S. J. Virulence plasmid harbored by uropathogenic Escherichia coli functions in acute stages of pathogenesis. *Infect. Immun.* **2010**, *7* (4), 1457−67.

(3) Litwin, C. M.; Calderwood, S. B. Role of iron in regulation of virulence genes. *Clin. Microbiol. Rev.* **1993**, *6* (2), 137−49.

(4) Torres, A. G.; Redford, P.; Welch, R. A.; Payne, S. M. TonB-dependent systems of uropathogenic Escherichia coli: aerobactin and heme transport and TonB are required for virulence in the mouse. *Infect. Immun.* **2001**, *69* (10), 6179−85.

(5) Hagan, E. C.; Mobley, H. L. Uropathogenic Escherichia coli outer membrane antigens expressed during urinary tract infection. *Infect. Immun.* **2007**, *75* (8), 3941−9.

(6) Dhakal, B. K.; Mulvey, M. A. The UPEC pore-forming toxin alpha-hemolysin triggers proteolysis of host proteins to disrupt cell adhesion, inflammatory, and survival pathways. *Cell Host Microbe* **2012**, *11* (1), 58−69.

(7) Watts, R. E.; Totsika, M.; Challinor, V. L.; Mabbett, A. N.; Ulett, G. C.; De Voss, J. J.; Schembri, M. A. Contribution of siderophore systems to growth and urinary tract colonization of asymptomatic bacteriuria Escherichia coli. *Infect. Immun.* **2012**, *80* (1), 333−44.

(8) Henderson, J. P.; Crowley, J. R.; Pinkner, J. S.; Walker, J. N.; Tsukayama, P.; Stamm, W. E.; Hooton, T. M.; Hultgren, S. J. Quantitative metabolomics reveals an epigenetic blueprint for iron acquisition in uropathogenic Escherichia coli. *PLoS Pathog.* **2009**, *5* (2), e1000305.

(9) Luo, M.; Lin, H.; Fischbach, M. A.; Liu, D. R.; Walsh, C. T.; Groves, J. T. Enzymatic tailoring of enterobactin alters membrane partitioning and iron acquisition. *ACS Chem. Biol.* **2006**, *1* (1), 29−32.

(10) Lv, H.; Henderson, J. P. Yersinia high pathogenicity island genes modify the Escherichia coli primary metabolome independently of siderophore production. *J. Proteome Res.* **2011**, *10* (12), 5547−54.

(11) Raymond, K. N.; Dertz, E. A.; Kim, S. S. Enterobactin: an archetype for microbial iron transport. *Proc. Natl. Acad. Sci. U.S.A.* **2003**, *100* (7), 3584−8.

(12) Miethke, M.; Marahiel, M. A. Siderophore-based iron acquisition and pathogen control. *Microbiol. Mol. Biol. Rev.* **2007**, *71* (3), 413−51.

(13) Neilands, J. B. Siderophores: structure and function of microbial iron transport compounds. *J. Biol. Chem.* **1995**, *270* (45), 26723−6.

(14) Griffin, A. S.; West, S. A. Buckling, A., Cooperation and competition in pathogenic bacteria. *Nature* **2004**, *430* (7003), 1024−7.

(15) Chaturvedi, K. S.; Hung, C. S.; Crowley, J. R.; Stapleton, A. E.; Henderson, J. P. The siderophore yersiniabactin binds copper to protect pathogens during infection. *Nat. Chem. Biol.* **2012**, *8* (8), 731−6.

(16) Chaturvedi, K. S.; Hung, C. S.; Giblin, D. E.; Urushidani, S.; Austin, A. M.; Dinauer, M. C.; Henderson, J. P. Cupric yersiniabactin is a virulence-associated superoxide dismutase mimic. *ACS Chem. Biol.* **2013**, DOI: 10.1021/cb400658k.

(17) Abdi, H.; Williams, L. J. Principal component analysis. *Wiley Interdiscip. Rev.: Comput. Stat.* **2010**, *2*, 433−459.

(18) Hantke, K.; Nicholson, G.; Rabsch, W.; Winkelmann, G. Salmochelins, siderophores of Salmonella enterica and uropathogenic Escherichia coli strains, are recognized by the outer membrane receptor IroN. *Proc. Natl. Acad. Sci. U.S.A.* **2003**, *100* (7), 3677−82.

(19) Snyder, J. A.; Haugen, B. J.; Buckles, E. L.; Lockatell, C. V.; Johnson, D. E.; Donnenberg, M. S.; Welch, R. A.; Mobley, H. L.

Transcriptome of uropathogenic Escherichia coli during urinary tract infection. *Infect. Immun.* **2004**, *72* (11), 6373−81.
(20) Alteri, C. J.; Mobley, H. L. Quantitative profile of the uropathogenic Escherichia coli outer membrane proteome during growth in human urine. *Infect. Immun.* **2007**, *75* (6), 2679−88.
(21) Fischbach, M. A.; Lin, H.; Liu, D. R.; Walsh, C. T. In vitro characterization of IroB, a pathogen-associated C-glycosyltransferase. *Proc. Natl. Acad. Sci. U.S.A.* **2005**, *102* (3), 571−6.
(22) Lin, H.; Fischbach, M. A.; Liu, D. R.; Walsh, C. T. In vitro characterization of salmochelin and enterobactin trilactone hydrolases IroD, IroE, and Fes. *J. Am. Chem. Soc.* **2005**, *127* (31), 11075−84.
(23) Abergel, R. J.; Moore, E. G.; Strong, R. K.; Raymond, K. N. Microbial evasion of the immune system: structural modifications of enterobactin impair siderocalin recognition. *J. Am. Chem. Soc.* **2006**, *128* (34), 10998−9.
(24) Fischbach, M. A.; Lin, H.; Zhou, L.; Yu, Y.; Abergel, R. J.; Liu, D. R.; Raymond, K. N.; Wanner, B. L.; Strong, R. K.; Walsh, C. T.; Aderem, A.; Smith, K. D. The pathogen-associated iroA gene cluster mediates bacterial evasion of lipocalin 2. *Proc. Natl. Acad. Sci. U.S.A.* **2006**, *103* (44), 16502−7.
(25) Sokol, P. A. Production and utilization of pyochelin by clinical isolates of Pseudomonas cepacia. *J. Clin. Microbiol.* **1986**, *23* (3), 560−2.
(26) Martin, L. W.; Reid, D. W.; Sharples, K. J.; Lamont, I. L. Pseudomonas siderophores in the sputum of patients with cystic fibrosis. *Biometals* **2011**, *24* (6), 1059−67.
(27) Bliven, K. A.; Maurelli, A. T. Antivirulence genes: insights into pathogen evolution through gene loss. *Infect. Immun.* **2012**, *80* (12), 4061−70.
(28) Winter, G.; Kromer, J. O. Fluxomics - connecting 'omics analysis and phenotypes. *Environ. Microbiol.* **2012**, *15*, 1901−16.
(29) Valdebenito, M.; Bister, B.; Reissbrodt, R.; Hantke, K.; Winkelmann, G. The detection of salmochelin and yersiniabactin in uropathogenic Escherichia coli strains by a novel hydrolysis-fluorescence-detection (HFD) method. *Int. J. Med. Microbiol.* **2005**, *295* (2), 99−107.
(30) Datsenko, K. A.; Wanner, B. L. One-step inactivation of chromosomal genes in Escherichia coli K-12 using PCR products. *Proc. Natl. Acad. Sci. U.S.A.* **2000**, *97* (12), 6640−5.
(31) Murphy, K. C.; Campellone, K. G. Lambda Red-mediated recombinogenic engineering of enterohemorrhagic and enteropathogenic E. coli. *BMC Mol. Biol.* **2003**, *4*, 11.
(32) Cherepanov, P. P.; Wackernagel, W. Gene disruption in Escherichia coli: TcR and KmR cassettes with the option of Flp-catalyzed excision of the antibiotic-resistance determinant. *Gene* **1995**, *158* (1), 9−14.
(33) Xia, J.; Psychogios, N.; Young, N.; Wishart, D. S. MetaboAnalyst: a web server for metabolomic data analysis and interpretation. *Nucleic Acids Res.* **2009**, *37* (Web Serverissue), W652−60.
(34) Xia, J.; Wishart, D. S. Web-based inference of biological patterns, functions and pathways from metabolomic data using MetaboAnalyst. *Nat. Protoc.* **2011**, *6* (6), 743−60.
(35) Tong, W.; Cao, X.; Harris, S.; Sun, H.; Fang, H.; Fuscoe, J.; Harris, A.; Hong, H.; Xie, Q.; Perkins, R.; Shi, L.; Casciano, D. ArrayTrack—supporting toxicogenomic research at the U.S. Food and Drug Administration National Center for Toxicological Research. *Environ. Health Perspect.* **2003**, *111* (15), 1819−26.
(36) Gehring, A. M.; DeMoll, E.; Fetherston, J. D.; Mori, I.; Mayhew, G. F.; Blattner, F. R.; Walsh, C. T.; Perry, R. D. Iron acquisition in plague: modular logic in enzymatic biogenesis of yersiniabactin by Yersinia pestis. *Chem. Biol.* **1998**, *5* (10), 573−86.
(37) Bachman, M. A.; Miller, V. L.; Weiser, J. N. Mucosal lipocalin 2 has pro-inflammatory and iron-sequestering effects in response to bacterial enterobactin. *PLoS Pathog.* **2009**, *5* (10), e1000622.